compared with the actual short and long reward times of the recording sessions, respectively (Fig. 3). Across recordings in experienced animals, the time (mean ± SEM) to the short reward was 1191 ± 35 ms; the mean left eye–dominated NRM was 1278 ± 42 ms. The time to the long reward was 1814 ± 84 ms; the mean right eye–dominated NRM was 1883 ± 116 ms. Therefore, on average, individual neurons predict reward time quite accurately.

The experience of pairing visual stimuli with delayed reward clearly alters the responses of V1 neurons to these visual cues while animals are performing the task. We next asked whether reward-timing activity would continue to be evoked by the same visual cues when the animals were not performing the task. After "within-task" recording sessions, access to the nose-poke/lick tube was obstructed, and the left and right eyes were stimulated pseudorandomly on a fixed 6-s interval until 180 presentations were reached for each stimulus, constituting "outside-task" sessions. By recording from the same neurons on a given day, we found that, of neurons expressing reward-timing activity within the task (47 out of 93; 51%), 66% (31 out of 47) continued to express apparent reward-timing activity to the visual stimuli when presented outside of the task (Fig. 4A). For these neurons, the accuracy with which they continued to "predict" the short and long reward times could be compared with their performance inside the task (Fig. 4B). Although neural timing of reward outside the task was degraded, left eye– and right eye–dominated neurons continued to have mean NRMs that were significantly different from each other ($P < 0.05$), relating to the appropriate reward times. This result indicates that pairing visual cues to delayed rewards within the task creates a lasting alteration in the manner in which the visual cortex responds to those cues when observed in other contexts. We hasten to add, however, that, although our data show that V1 responses evolve to accurately predict reward timing, further study is required to assess whether and how such information is used by the animal to guide behavior.

Such timing activity has been reported previously in higher cortical areas (*20*–*22*) and in associated subcortical structures (*23*–*25*), but never before in primary sensory cortex. The current findings imply that V1 neurons, at least in rats, do not function as simple feature detectors (*26*). Because reward-timing activity can persist long after the visual stimulus has disappeared, it no longer faithfully reports retinal illumination, but rather what retinal illumination portends. As reward timing is shown to be eye-specific, activating different subpopulations of neurons, general brain arousal/attention cannot explain this activity. Further, because these altered responses persist outside the task, emergent reward-timing activity can be independent of both context and behavior.

The mechanism for this remarkable plasticity in V1 remains to be determined. Subthreshold responses to stimulation of visual cortex, likely reflecting weak recurrent connections, can persist for seconds (*27*). Our findings could be explained if a modulatory input that signifies delivery of reward (possibly dopamine) causes a persistent potentiation or unmasking of recently active connections.

References and Notes

1. D. Hubel, T. Wiesel, *J. Physiol.* **150**, 91 (1959).
2. D. Hubel, T. Wiesel, *J. Physiol.* **160**, 106 (1962).
3. J. M. Fuster, G. E. Alexander, *Science* **173**, 652 (1971).
4. J. M. Fuster, *J. Neurophysiol.* **36**, 61 (1973).
5. E. K. Miller, C. A. Erickson, R. Desimone, *J. Neurosci.* **16**, 5154 (1996).
6. Y. Miyashita, H. S. Chang, *Nature* **331**, 68 (1988).
7. P. S. Goldman-Rakic, *Neuron* **14**, 477 (1995).
8. R. Desimone, *Proc. Natl. Acad. Sci. U.S.A.* **93**, 13494 (1996).
9. E. T. Rolls, *Cereb. Cortex* **10**, 284 (2000).
10. E. A. Gaffan, D. Gaffan, S. Harrison, *J. Neurosci.* **8**, 3144 (1988).
11. Z. Liu, E. A. Murray, B. J. Richmond, *Nat. Neurosci.* **3**, 1307 (2000).
12. M. R. Roesch, C. R. Olson, *J. Neurophysiol.* **90**, 1766 (2003).
13. Y. Tagawa, P. O. Kanold, M. Majdan, C. J. Schatz, *Nat. Neurosci.* **8**, 380 (2005).
14. N. B. Sawtell *et al.*, *Neuron* **38**, 977 (2003).
15. M. Ito, C. D. Gilbert, *Neuron* **22**, 593 (1999).
16. C. Gilbert, M. Ito, M. Kapadia, G. Westheimer, *Vision Res.* **40**, 1217 (2000).
17. H. Supèr, H. Spekreijse, V. A. Lamme, *Science* **293**, 120 (2001).
18. R. F. Salazar, P. Konig, C. Kayser, *Eur. J. Neurosci.* **20**, 1391 (2004).
19. Materials and Methods are available as supporting material on *Science* Online.
20. M. Leon, M. N. Shadlen, *Neuron* **38**, 317 (2003).
21. A. V. Egorov, B. N. Hamam, E. Fransen, M. E. Hasselmo, A. A. Alonso, *Nature* **420**, 173 (2002).
22. J. M. Fuster, J. P. Jervey, *Science* **212**, 952 (1981).
23. Y. Komura *et al.*, *Nature* **412**, 546 (2001).
24. W. Schultz, P. Dayan, P. R. Montague, *Science* **275**, 1593 (1997).
25. Y. Watanabe, S. Funahashi, *J. Neurophysiol.* **92**, 1738 (2004).
26. D. Purves, R. B. Lotto, S. M. Williams, S. Nundy, Z. Yang, *Philos. Trans. R. Soc. London B Biol. Sci.* **356**, 285 (2001).
27. M. V. Sanchez-Vives, D. A. McCormick, *Nat. Neurosci.* **3**, 1027 (2000).

28. This work was supported by the Howard Hughes Medical Institute. We thank R. Crozier, D. Foster, A. Heynen, M. Jones, D. Katz, J. Morgan, M. Linden, B. Rubin, and H. Shouval.

Supporting Online Material

www.sciencemag.org/cgi/content/full/311/5767/1606/DC1
Materials and Methods
SOM Text
Figs. S1 to S4
References and Notes

6 December 2005; accepted 13 February 2006
10.1126/science.1123513

αE-Catenin Controls Cerebral Cortical Size by Regulating the Hedgehog Signaling Pathway

Wen-Hui Lien,[1,2]* Olga Klezovitch,[1]* Tania E. Fernandez,[1] Jeff Delrow,[3] Valeri Vasioukhin[1]†

During development, cells monitor and adjust their rates of accumulation to produce organs of predetermined size. We show here that central nervous system–specific deletion of the essential adherens junction gene, *αE-catenin,* causes abnormal activation of the hedgehog pathway, resulting in shortening of the cell cycle, decreased apoptosis, and cortical hyperplasia. We propose that αE-catenin connects cell-density–dependent adherens junctions with the developmental hedgehog pathway and that this connection may provide a negative feedback loop controlling the size of developing cerebral cortex.

During brain development, proliferation of neural progenitor cells is tightly controlled to produce the organ of predetermined size. We hypothesized that cell-cell adhesion structures may be involved in this function, because they can provide cells with information concerning the density of their cellular neighborhood. Intercellular adhesion in neural progenitors is mediated primarily by adherens junctions, which contain cadherins, β-catenins and α-catenins (*1*). We found that progenitors express αE (epithelial)–catenin, while differentiated neurons express αN (neural)–catenin (fig. S1, A to D). Because α-catenin is critical for the formation of adherens junctions (*2*, *3*), we decided to determine the role of these adhesion structures in neural progenitor cells by generating mice with central nervous system (CNS)–specific deletion of *αE-catenin*. Mice with a conditional *αE-catenin* allele (*αE-catenin$^{loxP/loxP}$*) (*4*) were crossed with mice carrying nestin-promoter–driven Cre recombinase (*Nestin-Cre$^{+/-}$*), which

[1]Division of Human Biology, Fred Hutchinson Cancer Research Center, Seattle, WA 98109, USA. [2]Molecular and Cellular Biology Program, University of Washington, Seattle, WA 98195, USA. [3]Genomics Resource, Fred Hutchinson Cancer Research Center, Seattle, WA 98109, USA.

*These authors contributed equally to this work.
†To whom correspondence should be addressed. E-mail: vvasiouk@fhcrc.org

is expressed in CNS stem/neural progenitors starting at embryonic day 10.5 (E10.5) (fig. S1E) (*5*). The resulting *αE-catenin*$^{loxP/loxP}$*/Nestin-Cre*$^{+/-}$ animals displayed loss of αE-catenin in neural progenitor cells (fig. S1F).

Although no phenotype was observed in heterozygous *αE-catenin*$^{loxP/+}$*/Nestin-Cre*$^{+/-}$ mice, the knockout *αE-catenin*$^{loxP/loxP}$*/Nestin-Cre*$^{+/-}$ mice were born with bodies similar to their littermates, but with enlarged heads (fig. S2A). After birth, the heads of these animals continued to grow, but their bodies were developmentally retarded, generating abnormal large-headed pups that failed to thrive and died between 2 and 3 weeks of age (fig. S2B). Counting brain cell numbers at different points of embryonic development revealed massive hyperplasia in the mutant brains, with twice as many total brain cells by the time of birth (fig. S2C). Although no differences were found at E12.5, mutant brains displayed a 40% increase in total cell numbers only 1 day later at E13.5. In addition to an increase in brain cell numbers, the mutant animals displayed increases in brain weights and brain-to-body-weight ratios (fig. S2, D and E). Histologic analysis of *αE-catenin*$^{loxP/loxP}$*/Nestin-Cre*$^{+/-}$ animals revealed severe dysplasia and hyperplasia in the mutant brains (Fig. 1). *αE-catenin*$^{-/-}$ ventricular zone cells were dispersed throughout the developing brains, forming invasive tumor–like masses that displayed widespread pseudopalisading and the formation of rosettes (Fig. 1F′) similar to Homer-Wright rosettes in human medulloblastoma, neuroblastoma, retinoblastoma, pineoblastoma, neurocytoma, and pineocytoma tumors (*6*–*8*). Although E12.5 *αE-catenin*$^{-/-}$ cortices already showed some disorganization (Fig. 1B′), the general appearance of the brain was similar between the wild-type and *αE-catenin*$^{-/-}$ embryos (Fig. 1, A and A′). In contrast, the E13.5 mutants exhibited a prominent increase in the thickness and size of the cerebral cortex (Fig. 1, C and C′). Massive expansion of dysplastic cortical progenitor cells continued later in development, causing a posterior and ventral shift in localization of the lateral ventricle (Fig. 1, D to E′, and fig. S3).

We next analyzed the mechanisms responsible for dysplasia in *αE-catenin*$^{-/-}$ brains. Ventricular zone progenitors are bipolar, with one extension reaching the ventricular surface and another process reaching in the opposite direction (fig. S4A). These cells form a prominent cell-cell adhesion structure at the ventricular interface called an apical-junctional complex. Staining with cell adhesion and cell polarity markers showed disruption of apical-junctional complexes and loss of cell polarity in *αE-catenin*$^{-/-}$ neural progenitor cells (Fig. 2 and fig. S4). Electron microscopic analyses of *αE-catenin*$^{-/-}$ brains revealed progenitors that were nonpolarized, round, and loosely connected to each other and that lacked apical-junctional complexes (Fig. 2, G and H). Perhaps because of residual amounts of *αN-catenin* present in the progenitor cells, small fragments of *αE-catenin*$^{-/-}$ neuroepithelium were still capable of maintaining cell polarity, but they were often engulfed by protruding nonpolarized cells, folded back on themselves, and internalized to form rosettes (Fig. 2, D to F and I, and fig. S4, B and D). We concluded that loss of apical-junctional complexes and subsequent loss of cell polarity may represent the mechanism responsible for dysplasia in *αE-catenin*$^{-/-}$ brains.

We next analyzed the mechanisms responsible for hyperplasia in *αE-catenin*$^{-/-}$ brains. Failure of cell cycle withdrawal is responsible for hyperplasia in brains with hyperactive

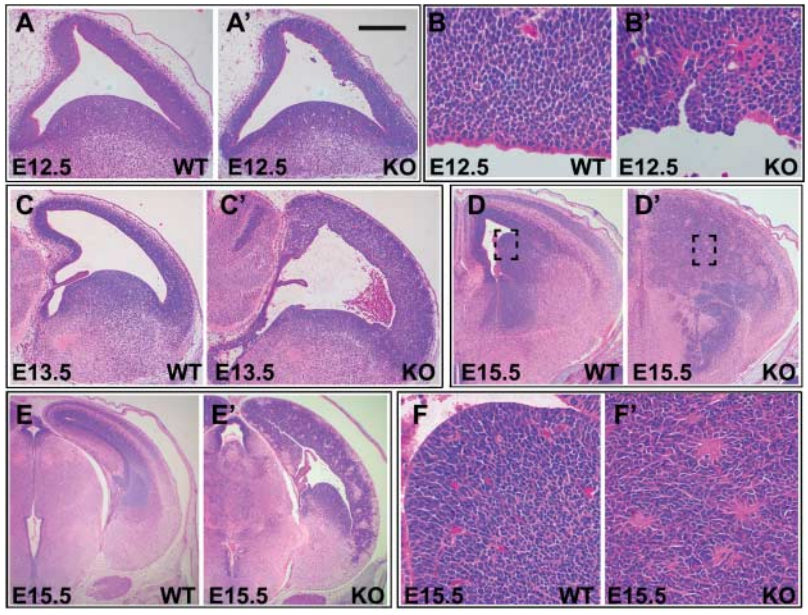

Fig. 1. Severe dysplasia and hyperplasia in *αE-catenin*$^{-/-}$ brain. Histologic appearance of brains from wild-type (WT) and *αE-catenin*$^{LoxP/LoxP}$*/Nestin-Cre*$^{+/-}$ (KO) mice. Sagittal sections through developing telencephalon from wild-type (**A** and **C**) and *αE-catenin*$^{-/-}$ (**A′** and **C′**) brains of E12.5 [(A) and (A′)] and E13.5 [(C) and (C′)] embryos. Ventricular zone of the cerebral cortex from the E12.5 wild-type (**B**) and *αE-catenin*$^{-/-}$ (**B′**) brains. Coronal sections from the E15.5 wild-type (**D** to **F**) and *αE-catenin*$^{-/-}$ (**D′** to **F′**) brains. Areas in dashed squares in (D) and (D′) are shown at higher magnification in (F) and (F′). Scale bar in (A′) represents 0.27 mm in (A) and (A′), 40 μm in (B) and (B′), 0.36 mm in (C) and (C′), 0.42 mm in (D) and (D′), 0.54 mm in (E) and (E′), and 50 μm in (F) and (F′).

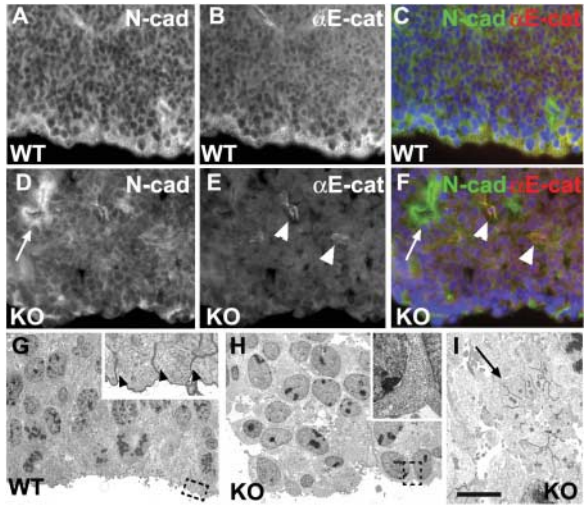

Fig. 2. Loss of cell polarity and disruption of apical-junctional complex in *αE-catenin*$^{-/-}$ neural progenitor cells. (**A** to **F**) Disruption of apical adherens junctions in *αE-catenin*$^{-/-}$ neural progenitors. Staining with antibody to N-cadherin [(A) and (D); green in (C) and F)] and antibody to αE-catenin [(B) and (E); red in (C) and F)]. (**G** to **I**) Electron microscopy analysis of cortical neural progenitor cells of E12.5 wild-type (G) and *αE-catenin*$^{-/-}$ [(H) and (I)] embryos. Areas in dashed squares in (G) and (H) are magnified in insets. Arrowheads in inset to (G) denote apical-junctional complexes. Arrows indicate internalization of polarized neuroepithelium and formation of rosettelike structures maintaining apical-junctional complexes. Arrowheads in (E) and (F) denote blood vessels not targeted by Nestin-Cre. Scale bar in (I) represents 30 μm in (A) to (F), 10 μm in (G) and (H), 4 μm in (I), and 1.8 μm in insets to (G) and (H).

β-catenin pathways (*9*). To analyze cell cycle withdrawal in *αE-catenin*$^{-/-}$ brains, we counted the proportion of cells that had exited the cell cycle 24 hours after labeling with 5-bromo-2′-deoxyuridine (BrdU) (Fig. 3, B and B′). We concentrated on E13.5 mutants, because we observed the most rapid increase in total brain cell numbers during the E12.5 to E13.5 interval of development. We found no significant differences in cell cycle withdrawal between the wild-type and mutant cells (Fig. 3C). To determine whether differentiation was affected in *αE-catenin*$^{-/-}$ brains, we used antibodies to β-tubulin III and nestin—neuronal and progenitor cell markers, respectively (fig. S5, A to B′). Although there were no differences in appearance of E12.5 wild-type and mutant cortices (fig. S5, A and A′), E13.5 *αE-catenin*$^{-/-}$ cortices were disorganized and thickened, with neurons present not only in the cortical plate but also elsewhere throughout the cortex (fig. S5, B and B′). Nevertheless, the overall ratio between differentiated and nondifferentiated cells remained unchanged (fig. S5C). Moreover, Western blot analyses of total brain proteins with cell type–specific antibodies did not reveal consistent differences between the wild-type and *αE-catenin*$^{-/-}$ brains (fig. S5D). In addition, we found no differences between the wild-type and *αE-catenin*$^{-/-}$ brains in the position and numbers of Cajal-Retzius neurons located at the surface of cerebral cortex (fig. S6). We concluded that, despite the loss of progenitor cell polarity, the general program governing differentiation is not affected in *αE-catenin*$^{-/-}$ brains.

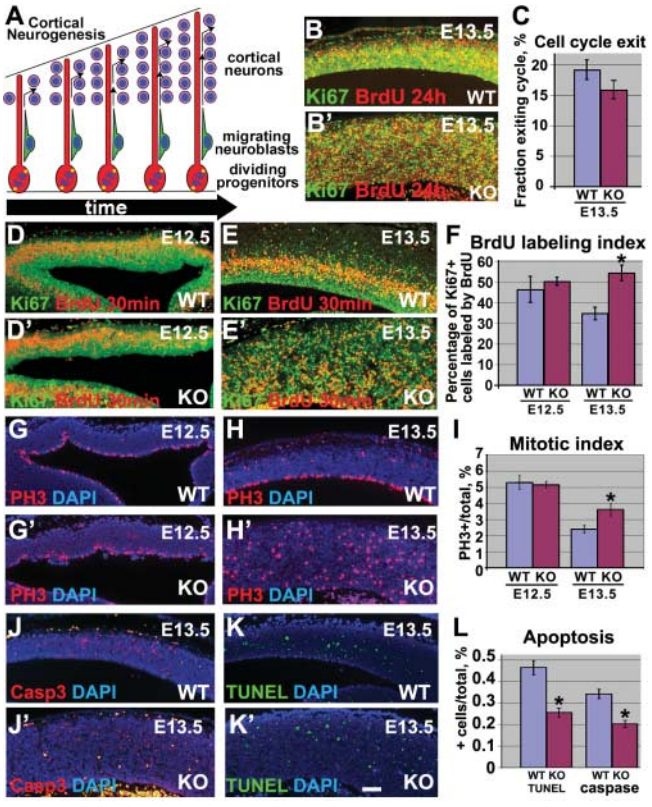

Fig. 3. Shortening of cell cycle and decreased apoptosis in *αE-catenin*$^{-/-}$ cerebral cortices. (**A**) Model of cortical neurogenesis. (**B** and **B′**) Minor changes in cell cycle withdrawal in *αE-catenin*$^{-/-}$ cortices. Pregnant females were injected with BrdU 24 hours before being sacrificed. Cells reentering the cell cycle are BrdU^{+}/Ki67^{+}, whereas cells withdrawn from the cell cycle are BrdU^{+}/Ki67^{-}. (**C**) Quantitation of experiments shown in (B) and (B′). Cell cycle exit is determined as a ratio of cells that exited the cell cycle (BrdU^{+}/Ki67^{-}) to all cells that incorporated BrdU. $n = 3$; (**D** to **E′**) Decrease in cell cycle length in *αE-catenin*$^{-/-}$ progenitors. A higher percentage of *αE-catenin*$^{-/-}$ progenitor cells (Ki67^{+}) are labeled with BrdU after a 30-min pulse. (**F**) Quantitation of experiments shown in (D) to (E′). BrdU labeling index is the percentage of Ki67^{+} cells that incorporated BrdU. $n = 3$; $^{*}P < 0.001$. (**G** to **H′**) Immunostaining of cortical sections from wild-type and *αE-catenin*$^{-/-}$ brains with antibodies to phosphohistone 3 (red) reveals an increase in mitotic cells in E13.5 mutants. DNA was counterstained by 4′,6′-diamidino-2-phenylindole (blue). (**I**) Quantitation of the experiments shown in (G) to (H′). Mitotic index is a ratio of mitotic cells to the total brain cell number. $n = 3$; $^{*}P < 0.001$. (**J** to **K′**) Decrease in apoptosis in *αE-catenin*$^{-/-}$ cortices. Apoptotic cells in the wild-type [(J) and (K)] and mutant [(J′) and K′)] brains were detected by staining with anti-body to cleaved caspase 3 (Casp3) and terminal deoxynucleotidyl transferase–mediated deoxyuridine triphosphate nick end labeling (TUNEL). (**L**) Quantitation of experiments shown in (J) and (K′). Ratios of Casp3^{+} or TUNEL^{+} cells to total cell numbers are shown. $n = 3$; $^{*}P < 0.001$. Scale bar in (K′) represents 100 μm in all cortical sections.

To analyze whether loss of αE-catenin led to changes in proliferation, we studied neural progenitor cell cycle length and number of cells in mitosis. To measure cell cycle length, we counted the proportion of neural progenitor cells labeled by a pulse of BrdU (*9*) (Fig. 3, D to E′). We found significant shortening of the cell cycle in E13.5 *αE-catenin*$^{-/-}$ progenitor cells (Fig. 3F). In addition, E13.5 mutant brains displayed a 40% increase in the number of mitotic cells (Fig. 3, G to I).

Apoptosis is also critical for regulation of total cell numbers in the developing brain (*10*). Counting of apoptotic cells revealed that apoptosis decreased by one-half in the *αE-catenin*$^{-/-}$ cortices (Fig. 3, J to L). We concluded that hyperplasia in the *αE-catenin*$^{-/-}$ brains was a combined outcome of the shortening of the cell cycle and the decreased apoptosis in neural progenitor cells.

To determine the molecular mechanisms responsible for hyperplasia in *αE-catenin*$^{-/-}$ brains, we used a microarray approach. Surprisingly, a genomewide analysis revealed few changes in gene expression (Table 1),

Table 1. Differentially expressed genes in E12.5 αE-catenin$^{-/-}$ brains. RNAs from *αE-catenin*$^{LoxP/+}$*/Nestin-Cre*$^{+/-}$ and *αE-catenin*$^{LoxP/LoxP}$*/Nestin-Cre*$^{+/-}$ brains were analyzed by Affymetrix expression arrays. Relative fold change is calculated with respect to heterozygous brains. Bayes.p is the *P* value obtained using the CyberT Bayesian statistical framework.

Name	Symbol	UG cluster	Relative fold change	Bayes.p
Up-regulated				
Fibroblast growth factor 15	Fgf15	Mm.3904	2.39	1.31×10^{-6}
GLI-Kruppel family member GLI	Gli1	Mm.336839	2.37	3.34×10^{-6}
RIKEN cDNA A830059I20 gene	A830059I20Rik	Mm.113787	1.98	5.86×10^{-7}
Expressed sequence AU040576	AU040576	Mm.26700	1.93	2.27×10^{-5}
High mobility group AT-hook 1	Hmga1	Mm.4438	1.59	1.60×10^{-5}
Down-regulated				
p53 binding protein 1	Trp53bp1	Mm.215389	−3.91	6.70×10^{-6}
RIKEN cDNA 2900097C17 gene	2900097C17Rik	Mm.349235	−2.63	5.41×10^{-6}
RIKEN cDNA A730017C20 gene	A730017C20Rik	Mm.209711	−1.92	2.55×10^{-7}

with only five transcripts up-regulated and three down-regulated in *αE-catenin*$^{-/-}$ brains. Interestingly, the two most up-regulated cDNAs, *Fgf15* and *Gli1*, represent well-known endogenous transcriptional targets of the hedgehog (Hh) pathway (*11*, *12*). We performed quantitative reverse transcription polymerase chain reaction (PCR) analysis of critical members and targets of the Hh pathway: *smoothened* (*Smo*), *patched1* (*Ptch*), *sonic hedgehog* (*Shh*), *indian hedgehog* (*Ihh*), *desert hedgehog* (*Dhh*), *Rab23*, *Gli1*, *Gli2*, *Gli3*, and *Fgf15*. We found that the expression of *Gli1*, *Fgf15*, and *Smo* was significantly up-regulated in *αE-catenin*$^{-/-}$ brains (Fig. 4A). To determine the compartment of the developing brain displaying up-regulation of Hh signaling, we performed in situ hybridizations with *Gli1*, *Fgf15*, and *Smo* probes (Fig. 4, B to D′). We found that *Gli1* and *Fgf15* transcripts are up-regulated in the progenitor cell domain of *αE-catenin*$^{-/-}$ cerebral cortex, the area most severely affected by hyperplasia in *αE-catenin*$^{-/-}$ brains (Fig. 1C′).

Up-regulation of endogenous targets of the Hh signaling pathway suggests activation of this pathway in developing cortices of the *αE-catenin*$^{loxP/loxP}$*/Nestin-Cre*$^{+/-}$ mice. Although the exact mechanism responsible for αE-catenin–mediated regulation of *Gli1* and *Fgf15* is presently unknown, an increase in expression of the activator of the Hh signaling *Smo* is likely to play a causal role in abnormal activation of the Hh pathway in *αE-catenin*$^{-/-}$ brains. Indeed, *Smo* up-regulation is responsible for activation of Hh signaling in cancer cell lines, and it may be a focal point of regulation of the pathway in tissue regeneration and cancer (*13*).

The Hh pathway plays a critical role in mammalian CNS development and brain cancer (*14*). Sonic hedgehog stimulates proliferation of progenitor cells in the developing cerebral cortex (*15*, *16*). In addition, Hh signaling promotes survival and blocks apoptosis of neuroepithelial cells (*17*). Therefore, abnormal activation of the Hh pathway may be responsible for cortical hyperplasia in *αE-catenin*$^{-/-}$ brains. To determine whether this is indeed the case, we used cyclopamine, a specific inhibitor of Smoothened (*18*), which can block the Hh pathway in vivo (*19*). We found that a single injection of cyclopamine at E12.5 (immediately before the onset of hyperplasia) did not interfere with depletion of αE-catenin (fig. S7) but eliminated the differences in total cell numbers between the E13.75 wild-type and *αE-catenin*$^{-/-}$ brains (Fig. 4E). Injections of decreasing amounts of cyclopamine produced intermediate phenotypes demonstrating dose dependence between the inhibitor and hyperplasia (fig. S8). As expected, inhibition of Hh did not rescue cortical disorganization, which results from the disruption of adherens junctions in *αE-catenin*$^{-/-}$ brains (fig. S9). Analyses of the cell cycle length and apoptosis showed rescue of the cell cycle and apoptosis abnormalities in cyclopamine-treated *αE-catenin*$^{-/-}$ brains (Fig. 4E and fig. S9, C to H′). As expected, cyclopamine injection led to a decrease in expression of the Hh pathway transcriptional targets *Gli1* and *Fgf15* (fig. S10). We concluded that abnormal activation of the Hh pathway was responsible for shortening of the cell cycle, decreased apoptosis, and subsequent hyperplasia in *αE-catenin*$^{-/-}$ cerebral cortices.

Our findings allow us to propose a model of a negative feedback loop that regulates the rates of cell proliferation to control the size of the cerebral cortex (fig. S11). In this "crowd control" model, the increase in cell density, which is sensed by an increase in the per cell area occupied by adherens junctions (fig. S11A), is translated into down-regulation of Hh signaling and subsequent decrease in cell proliferation (fig. S11B). The abnormal decrease in cell density, which is measured by destabilization and paucity of adherens junctions, is translated into activation of the Hh pathway and subsequent acceleration of cell proliferation until the normal cell density is achieved. Therefore, the density of cellular crowding ultimately regulates the rates of cell accumulation during normal development. Solid tumors may escape "crowd control" of cell proliferation by destabilizing the adherens junctions, one of the frequent events reported in human cancers (*20*).

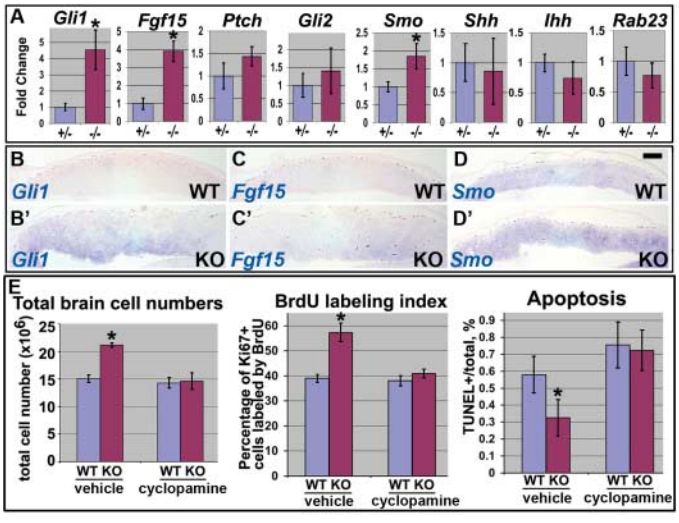

Fig. 4. Activation of the Hh pathway is responsible for shortening of the cell cycle, decreased apoptosis, and subsequent hyperplasia in *αE-catenin*$^{-/-}$ cerebral cortices. (**A**) Quantitative real-time PCR (QPCR) analysis of Hh pathway transcripts in E12.5 heterozygous and mutant brains. The levels of expression are shown in arbitrary units, with mean heterozygous levels adjusted to 1. Data represent mean ± SD. $n \geq 4$; *$P < 0.002$. (**B** to **D′**) Cortical sections from E12.5 wild-type and αE-catenin$^{-/-}$ embryos were analyzed by in situ hybridization with *Gli1*, *Fgf15*, and *Smo* probes. Scale bar in (D) represents 200 μm. (**E**) Inhibition of the Hh pathway by cyclopamine eliminates the differences in total cell numbers, cell cycle length, and apoptosis between the wild-type and *αE-catenin*$^{-/-}$ brains. Pregnant females were injected with 10 mg of cyclopamine per kg of body weight in 2-hydropropyl-β-cyclodextrin (vehicle) or vehicle alone at E12.5, and embryos were analyzed 30 hours later. Quantitation was performed as described in Fig. 3 and fig. S2. Data represent mean ± SD. $n \geq 3$; *$P < 0.001$.

References and Notes

1. A. Chenn, Y. A. Zhang, B. T. Chang, S. K. McConnell, *Mol. Cell. Neurosci.* **11**, 183 (1998).
2. S. Hirano, N. Kimoto, Y. Shimoyama, S. Hirohashi, M. Takeichi, *Cell* **70**, 293 (1992).
3. V. Vasioukhin, C. Bauer, M. Yin, E. Fuchs, *Cell* **100**, 209 (2000).
4. V. Vasioukhin, C. Bauer, L. Degenstein, B. Wise, E. Fuchs, *Cell* **104**, 605 (2001).
5. D. Graus-Porta *et al.*, *Neuron* **31**, 367 (2001).
6. O. P. Sangueza, P. Sangueza, L. R. Valda, C. K. Meshul, L. Requena, *J. Am. Acad. Dermatol.* **31**, 356 (1994).
7. D. I. Graham, P. L. Lantos, *Greenfield's Neuropathology* (Arnold, New York, NY, 2002).
8. P. C. Burger, Scheithauer, *Atlas of Tumor Pathology. Tumors of the Central Nervous System* (Armed Forces Institute of Pathology, Washington, DC, 1994).
9. A. Chenn, C. A. Walsh, *Science* **297**, 365 (2002).
10. V. Depaepe *et al.*, *Nature* **435**, 1244 (2005).
11. M. Ishibashi, A. P. McMahon, *Development* **129**, 4807 (2002).
12. H. Saitsu *et al.*, *Dev. Dyn.* **232**, 282 (2005).
13. S. S. Karhadkar *et al.*, *Nature* **431**, 707 (2004).
14. A. Ruiz i Altaba, V. Palma, N. Dahmane, *Nat. Rev. Neurosci.* **3**, 24 (2002).
15. N. Dahmane *et al.*, *Development* **128**, 5201 (2001).
16. V. Palma, A. Ruiz i Altaba, *Development* **131**, 337 (2004).
17. C. Thibert *et al.*, *Science* **301**, 843 (2003).
18. J. K. Chen, J. Taipale, M. K. Cooper, P. A. Beachy, *Genes Dev.* **16**, 2743 (2002).
19. D. M. Berman *et al.*, *Science* **297**, 1559 (2002).
20. U. Cavallaro, G. Christofori, *Nat. Rev. Cancer* **4**, 118 (2004).

21. We thank P. Soriano, S. Parkhurst, S. Tapscott, D. Gottschling, B. Edgar, and all members of the Vasioukhin laboratory for advice and encouragement; A. Nagafuchi, S. Tsukita, and the Developmental Studies Hybridoma Bank for the generous gift of antibodies; and L. Cherepoff, F. Remington, M. Null, and B. Helbing for help with histology, electron microscopy, genotyping, and manuscript preparation, respectively. This work was supported by National Cancer Institute grant R01 CA098161.

Supporting Online Material

www.sciencemag.org/cgi/content/full/311/5767/1609/DC1
Materials and Methods
Figs. S1 to S11
References

17 October 2005; accepted 31 January 2006
10.1126/science.1121449